Available online at www.sciencedirect.com
ScienceDirect
Journal of Power Sources 179 (2008) 848–853
JOURNAL OF POWER SOURCES
www.elsevier.com/locate/jpowsour

Short communication

Numerical simulation and optimization of nickel–hydrogen batteries

Li-Jun Yu [a,*], Ming-Jun Qin [a], Peng Zhu [a], Li Yang [b]

[a] *Institute of Thermal Energy Engineering, Shanghai Jiao Tong University, Shanghai 200240, China*
[b] *Department of Chemistry, Shanghai Jiao Tong University, Shanghai 200240, China*

Received 19 June 2007; accepted 15 December 2007
Available online 20 January 2008

Abstract

A three-dimensional, transient numerical model of an individual pressure vessel (IPV) nickel–hydrogen battery has been developed based on energy conservation law, mechanisms of heat and mass transfer, and electrochemical reactions in the battery. The model, containing all components of a battery including the battery shell, was utilized to simulate the transient temperature of the battery, using computational fluid dynamics (CFD) technology. The comparison of the model prediction and experimental data shows a good agreement, which means that the present model can be used for the engineering design and parameter optimization of nickel–hydrogen batteries in aerospace power systems. Two kinds of optimization schemes were provided and evaluated by the simulated temperature field. Based on the model, the temperature simulation during five successive periods in a designed space battery was conducted and the simulation results meet the requirement of safe operation.

Keywords: Nickel–hydrogen battery; Computational fluid mechanics; Transient model; Numerical simulation; Temperature field

1. Introduction

Nickel–hydrogen technology is originally built up around individual pressure vessel (IPV) designs. Since 1983, there has been a gradual shift away from nickel–cadmium to nickel–hydrogen energy storage by many space programs [1]. The nickel–hydrogen battery is a desirable alternative for traditional batteries due to its higher energy density, high rate capability, long cycle life, and free of poisonous materials [2]. However, the nickel–hydrogen batteries retain huge heat and less uninformed temperature profiles under large loads or rapid charge/discharge, seriously leading to the performance fade [3]. Battery failure could also result from excessive temperature rise and steeper temperature gradient within a battery [4]. Therefore, it is of primary importance to study the temperature field of nickel–hydrogen batteries.

Traditionally, experimental testing is a main tool to test and design batteries. However, experiments are time consuming and costly, and experimentally it is difficult to determine the internal process during charge and discharge [2]. With the rapid development of computer technology, modeling and simulation have become an indispensable approach in the design and optimization of many engineering systems [5]. Modeling and simulation are powerful methods for identifying battery mechanisms, predicting the cell performance for design and optimization, and reducing the cost and time expended on the experiments. Gu et al. [6] constructed a three-phase electrochemical model for nickel–metal hydride cells using the micromacroscopic coupled approach. Shi et al. [3] developed a two-dimensional thermal model to predict the temperature distribution of cylindrical 8-Ah Ni/MH battery. However, there are few publications on three-dimensional thermal model of IPV batteries for analysis and design.

In the present work, a three-dimensional, transient thermal model of an IPV nickel–hydrogen battery was constructed for simulating and analyzing the temperature field of the battery with different design and operational conditions.

Abbreviations: IPV, individual pressure vessel; CFD, computational fluid dynamics.

* Corresponding author. Tel.: +86 21 3420 6287; fax: +86 21 3420 5681.
E-mail address: ljyu@sjtu.edu.cn (L.-J. Yu).

0378-7753/$ – see front matter © 2008 Elsevier B.V. All rights reserved.
doi:10.1016/j.jpowsour.2007.12.126

Nomenclature

c	specific heat ($J\,kg^{-1}\,K^{-1}$)
E	battery voltage (V)
E_H	heat value voltage of battery (1.508 V)
F	Faraday constant (96,487 $C\,mol^{-1}$)
ΔH_R	enthalpy of charging reactions (145.50kJ mol^{-1})
ΔH_{SR}	enthalpy of charging side reactions (285.83 kJ mol^{-1})
I	total current (A)
I_d	total discharge current (A)
n	amount of gain and loss electrons in electrochemical reactions
P	pressure of battery cavity (atm)
q_0	heat-generation rate by oxygen recombination (W)
Q	energy source item ($W\,cm^{-3}$)
t	time (s)
T	temperature (K)
V	volume of battery cavity (m^3)
V_d	operation voltage (V)
V_{Ni}	volume of nickel electrode (m^3)

Greek letters

η	charging current efficiency
λ	thermal conductivity ($W\,cm^{-1}\,K^{-1}$)
ρ	density ($kg\,cm^{-3}$)

2. Operational principle and geometric model of the IPV nickel–hydrogen battery

2.1. Operational principle of the IPV nickel–hydrogen battery

"Back to back" stacking arrangement was used in the IPV nickel–hydrogen battery [1]. The electrode stack was contained in a sealed pressure vessel that was filled with certain-pressure hydrogen gas. Fig. 1 shows the structure of an electrode stack.

Shown in Fig. 1, the electrode stack is surrounded by hydrogen gas. The positive nickel electrode is filled with electrolyte in its pore structure. The negative platinum electrode is filled with hydrogen gas in its spacing. The polypropylene separator filled with electrolyte is placed between the nickel and platinum electrodes.

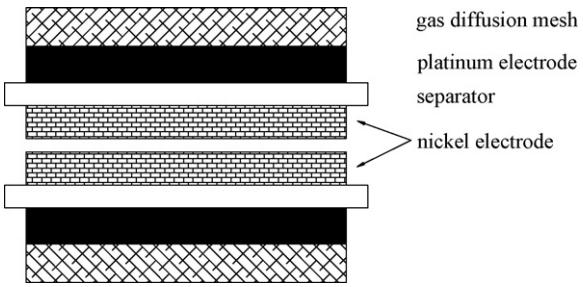

Fig. 1. Schematic diagram of an electrode stack.

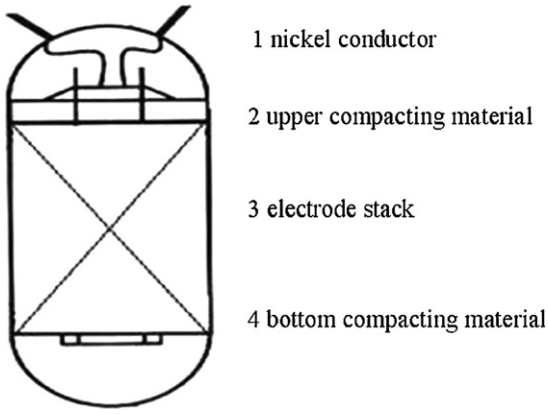

Fig. 2. Framework of an IPV battery.

Electrochemical reactions in the nickel–hydrogen battery are given below [1,5,7,8]:

At the nickel electrode $NiOOH + H_2O + e^- \underset{\text{charge}}{\overset{\text{discharge}}{\rightleftharpoons}} Ni(OH)_2 + OH^-$ (1)

with the side reaction $2OH^- \rightarrow \frac{1}{2}O_2 + H_2O + 2e^-$ (2)

At the platinum electrode $\frac{1}{2}H_2 + OH^- \underset{\text{charge}}{\overset{\text{discharge}}{\rightleftharpoons}} H_2O + e^-$ (3)

with the side reaction $\frac{1}{2}O_2 + H_2O + 2e^- \rightarrow 2OH^-$ (4)

Net reactions within the battery $NiOOH + \frac{1}{2}H_2 \underset{\text{charge}}{\overset{\text{discharge}}{\rightleftharpoons}} Ni(OH)_2$ (5)

2.2. Geometric model of the IPV nickel–hydrogen battery

Generally, the electrode stack of an IPV nickel–hydrogen battery is composed of back-to-back single chip cells that are in turn connected in parallel [1]. The electricity generated from the electrochemical reactions is conducted outside by its nickel conductor. Fig. 2 shows the framework of an IPV nickel–hydrogen battery. The components of an IPV nickel–hydrogen battery as shown include (from top to bottom) nickel conductor (pos. 1), upper compacting material (pos. 2), the electrode stack (pos. 3), bottom compacting material (pos. 4), with the rest areas full of hydrogen gas.

The electrode stack of a nickel–hydrogen battery consists of 26 single chip cells, with a gas diffusion mesh between every two single chip cells. The physical and thermal properties of electrode stack and shell is listed in Table 1. The materials and some physical aspects of a single chip cell are given in Table 2.

In fact, internal configuration of an actual IPV nickel–hydrogen battery is more complex. Polysulfone materials and internal nickel conductor both have irregular structures. Much spacing exists in the interior electrode stack

Table 1
Physical and thermal properties of electrode stack and shell

	Amount	Single thickness (mm)	Spacing ratio %	Sizes (outside/inside diameter)
Anode plaque	26	0.88	23	85/26.5
Cathode plaque	26	0.13	15	84/26.5
Diffusion mesh	14	0.617	41	85/26
Separator	104	0.096	73	87.6/25
Wall zirconia	–	0.1	–	87.8/87.6
Battery shell	–	0.6	–	89/87.8

Table 2
Materials and physical aspects of a single chip cell

	Specification	Spacing ratio %	Thermal conductivity ($W\,cm^{-1}\,k^{-1}$)
Anode plaque	Nickel electrode with electrolyte filled in its pore structure	23	0.329
Cathode plaque	Platinum electrode with hydrogen gas filled in its spacing	15	6.3243
Diffusion mesh	Polypropylene screen with hydrogen gas filled in its spacing	41	1.5226
Separator	Polypropylene with electrolyte filled in its spacing	73	
Battery shell	Inconel718	–	1.470
Compacting materials	Polysulfone [9]	–	1

and the battery shell consists of several different kinds of materials.

3. Numerical model of the nickel–hydrogen battery

Heat conduction is governed by energy conservation law:

$$\frac{\partial(\rho c T)}{\partial t} = \mathrm{div}(\lambda\,\mathrm{grad}\,T) + Q \tag{6}$$

here ρ denotes density, while c signifies specific heat, λ indicates thermal conductivity, T is the temperature, Q is the energy source item, and t is the time. We can respectively employ Eq. (6) to each component within the battery and obtain numerical solution by finite volume method.

The energy source items of the battery components, except the nickel electrode, all take a value of zero to show that there is no internal thermal source. The value of Q for the nickel electrode can be calculated as follows [10]:

$$Q = \frac{(E_H - V_d)I_d}{V_{Ni}} \tag{7}$$

In Eq. (7), E_H is the heat value voltage of the battery (1.508 V), V_d is the operation voltage, I_d is the total discharging current, and V_{Ni} is the volume of the nickel electrode.

First, two assumptions are made as given below:

(1) The reactions take place in isochoric process without any change of kinetic or thermal energy.
(2) The process of discharging has no side reactions, while the current efficiency influenced by side reactions during the charging process should be considered.

So the expression for heat change is obtained, as

$$\frac{dQ}{dt} = \frac{\Delta H_R}{nF}\eta I + \frac{\Delta H_{SR}}{nF}(1-\eta)I - V\frac{dP}{dt} - EI - q_0 \tag{8}$$

here $\Delta H_R/nF = 1.508$ V, V stands for the volume of battery cavity, I is the total current, E is the battery voltage, ΔH_R is the enthalpy of charging reactions (145.50 KJ mol^{-1}), η is the charging current efficiency, ΔH_{SR} is the enthalpy of charging side reactions (285.83 KJ mol^{-1}), t is the time, P is the pressure of battery cavity, q_0 is heat-generation rate by oxygen recombination, F is Faraday constant (96,487 C mol^{-1}), and n is the amount of gain and loss electrons in electrochemical reactions.

And then it is further assumed, as: (3) the production and recombination of oxygen during the process of charging side reaction have the same rate, so $(\Delta H_{SR}/nF)(1-\eta)I$ counteracts the value of q_0.

Thus, the equation for the heat generation rate during charge is obtained as follows:

$$q_{charge} = -\frac{dQ}{dt} = I\left(E - \frac{\Delta H_R}{nF}\eta\right) + V\frac{dP}{dt} \tag{9}$$

as well as the equation for the heat generation rate during discharge:

$$q_{discharge} = -\frac{dQ}{dt} = I\left(\frac{\Delta H_R}{nF}\eta - E\right) + V\frac{dP}{dt}. \tag{10}$$

4. Comparison and analysis of the simulation results

With the aid of computational fluid dynamics (CFD), we conducted a numerical simulation of the IPV nickel–hydrogen battery model described above and compared it with the experimental data (see the figures below) from XXX Institute of Space Power Sources, including temperature–time curve of different components: the upper acme (see Fig. 3), the nether acme (see Fig. 4), the jointing circle (see Fig. 5) and the stack (see Fig. 6). As can be seen, the simulation results match the experimental data well.

According to the numerical simulation, it is indicated that the maximum temperature during the operation occurs in the middle stack and the minimum temperature appears at the nether acme.

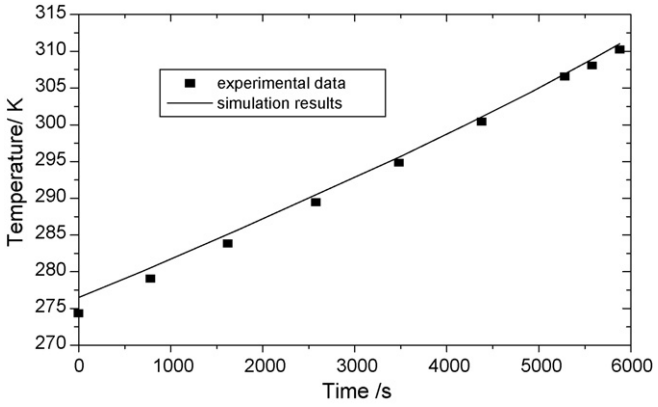

Fig. 3. Temperature–time curve of the upper acme (comparison between simulation results and experimental data).

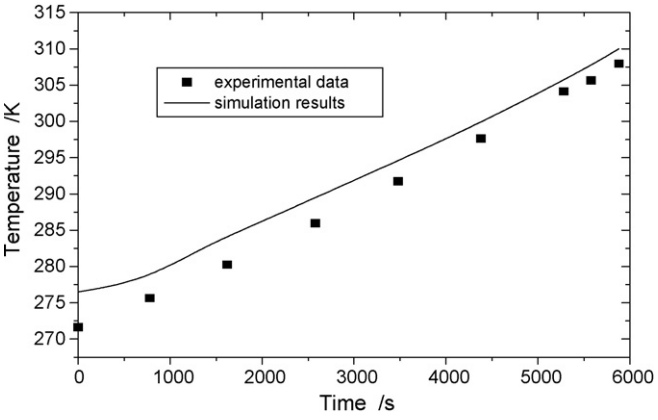

Fig. 4. Temperature–time curve of the nether acme (comparison between simulation results and experimental data).

The largest temperature difference in the battery is 5.3 K, which meets the requirement for safe operation.

The simulation errors of temperature distribution in the nether acme, middle section and nether section of the electrode stack are all less than 2 K, while that of the upper acme partially excesses 3 K. However, all the errors are within the permitted range and the model can still well describe the battery temperature field.

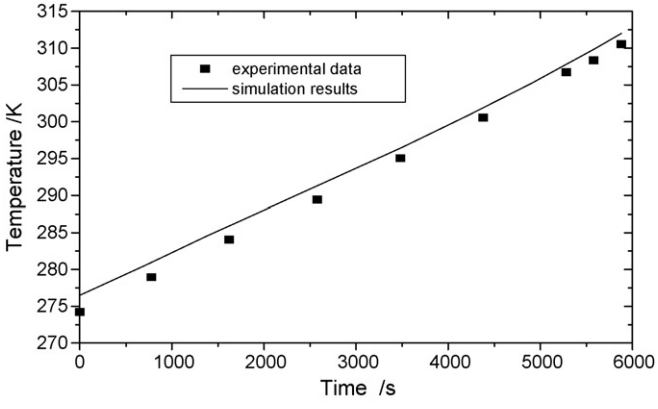

Fig. 5. Temperature–time curve of the jointing circle (comparison between simulation results and experimental data).

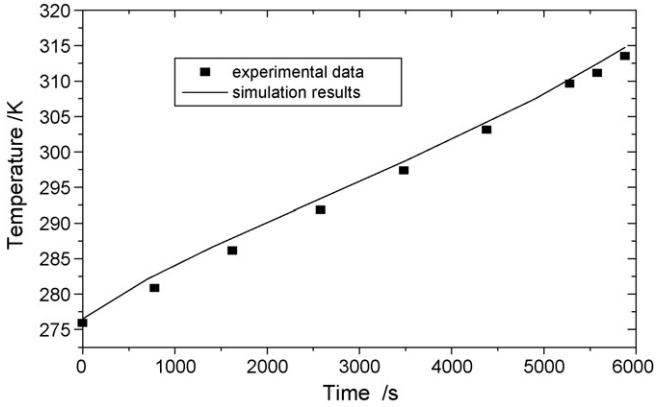

Fig. 6. Temperature–time curve of the stack (comparison between simulation results and experimental data).

On the basis of the comparison of the discharging experimental data in the adiabatic process with the simulation results, an accurate, three-dimension, transient numerical model of the battery was constructed. It can be used for the engineering design and parameter optimization of IPV nickel–hydrogen batteries in aerospace power system.

5. Optimization schemes and simulation results

In order to obtain more useful guidance for battery design, the discrepancy in temperature fields of nickel–hydrogen batteries with different configurations should be considered and thus optimization simulation for the battery is necessitated.

Two kinds of optimization schemes for battery configuration were adopted as follows:

(1) Only the location of the stack was changed, while the shapes of the battery shell, compacting materials, electrical terminals and the stack remained the same. Thus the influence of different positions on temperature distribution can be found. Shown in Tables 3 and 4 are the simulated temperature contribution when the stack is in the middle and at the bottom, respectively.

From Tables 3 and 4, it can be concluded that the largest temperature differences across the battery when the stack is

Table 3
Simulated temperatures of different components (when the stack is in the middle of the battery)

Time (min)	Upper acme (K)	Stack (K)	Nether acme (K)
0	276.5	276.5	276.5
10	278.8	280.4	278.5
20	282.2	284.1	281.7
30	285.7	287.7	285.1
40	289.2	291.2	288.6
50	292.8	294.98	292.13
60	296.3	298.7	295.75
70	300.3	302.3	299.48
80	304.3	306.3	303.4
90	308.6	310.6	307.5
98	312.2	314.5	311.1

Table 4
Simulated temperatures of different components (when the stack is at the bottom of the battery)

Time (min)	Upper acme (K)	Stack (K)	Nether acme (K)
0	276.5	276.5	276.5
10	278.8	280.0	278.1
20	281.3	284.12	280.8
30	285.7	287.6	284.1
40	289.02	291.08	287.42
50	293.0	295.1	291.3
60	297.0	298.57	294.67
70	300.1	302.34	298.32
80	305.6	307.5	303.2
90	309.2	311.6	306.83
98	312.1	314.38	309.69

Table 5
Simulated temperatures of different components (when the inside diameter of the stack is 19.5 mm)

Time (min)	Upper acme (K)	Stack (K)	Nether acme (K)
0	276.5	276.5	276.5
10	278.89	280.46	278.72
20	282.4	284.16	282
30	285.88	287.79	285.42
40	289.45	291.435	288.96
50	293	295.11	292.6
60	296.68	298.86	296.24
70	300.51	302.73	300.04
80	304.5	306.79	304
90	308.7	311.13	308.21
98	312.43	314.88	311.82

placed in the middle and at the bottom are 3.4 and 4.69 K, respectively. What's more, the temperature field is much better while the stack is in the middle of the battery.

(2) The shape of the battery shell and the volume of the stack remained the same and the stack was in the middle of the battery all the time. Thus the temperature distribution under different inside diameters of the stack can be simulated numerically. Tables 3, 5, and 6 show the simulation results under three inside diameters: 13, 19.5 and 6.5 mm, respectively.

Table 6
Simulated temperatures of different components (when the inside diameter of the stack is 6.5 mm)

Time (min)	Upper acme (K)	Stack (K)	Nether acme (K)
0	276.5	276.5	276.5
10	278.1	280.8	278.0
20	282.0	284.4	281.7
30	285.7	288.1	285.0
40	289.4	291.9	288.5
50	293	295.6	292.3
60	297.1	299.3	296.44
70	300.31	303.1	299.74
80	304.4	307.1	303.6
90	308.9	311.5	307.4
98	312.33	314.7	310.8

In Tables 3, 5 and 6, for the three inside diameters of the stack, the largest temperature differences are 3.4, 3.02 and 3.9 K, respectively. The temperature difference decreases when the length of inside diameter of the stack increases. In sum, as long as keeping the stack in the middle of the battery, the longer the inside diameter is, the smaller largest temperature difference the battery gets.

6. Analysis of periodic charge/discharge behaviors of the nickel–hydrogen battery

When the IPV nickel–hydrogen battery is practically used in aerospace power system, it must be assured that the temperature field of the battery meets the requirement for safe operation under successive charge and discharge. This model can be used to simulate such successive periodic temperature field of the battery.

The charging current of a designed space IPV battery is 16 A and the charging process lasts 50 min. Its discharging current is 20 A and the process lasts 37 min. The voltages of successive five-period charge/discharge are shown in Fig. 7.

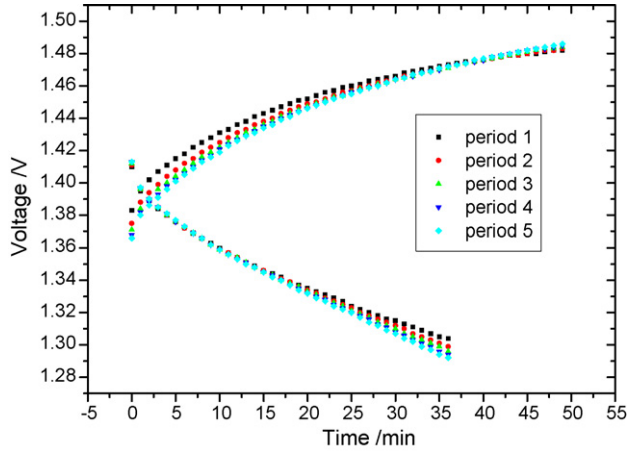

Fig. 7. Charging/discharging voltages of the battery during successive five periods.

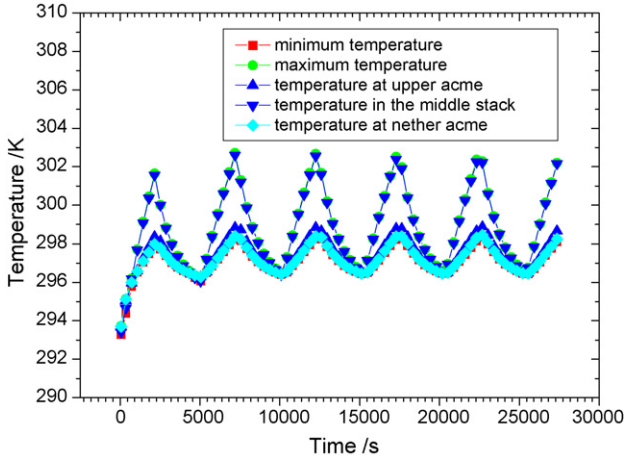

Fig. 8. Simulated temperature–time curve during successive five periods.

The simulation of the temperature field for successive five-period charge/discharge in a designed space battery was conducted. Fig. 8 shows that the largest temperature differences within the battery are all less than 5 K at any time during the continuous five periods. At 7200 s, the maximum temperature throughout the battery occurs in the middle of the stack and the minimum temperature appears at the nether acme. The largest temperature difference reaches the maximum value, 4.44 K. Therefore, it can be concluded that the configuration of the IPV nickel–hydrogen battery is reasonably designed and meets the requirement of safe design and operation.

7. Conclusions

A three-dimensional, transient numerical model of an IPV hydrogen battery was developed with attention given to many important mechanisms in the battery. This model includes nearly all the parts of a battery, such as the battery shell, electrode stack, nickel conductor and hydrogen gas area, etc. By using CFD technology, the model was used to numerically simulate the transient temperature of an IPV battery and the simulation results fit the experimental data well. Two kinds of optimization schemes were provided and evaluated by the simulation temperature field. With the temperature field simulation, the influence of interior structure on temperature was studied while the positions of the maximum and minimum temperatures were ascertained. And the largest temperature differences of the battery from the calculation can be helpful for effectively analyzing the operational condition of the battery. Overall, this accurate, three-dimensional, transient numerical model can be used for the engineering design and parameter optimization of nickel–hydrogen batteries in aerospace power systems.

Acknowledgement

This project was financially supported by National Natural Science Foundation of China (No. 50676058).

References

[1] L.H. Thaller, A.H. Zimmerman, Overview of the Design, Development, and Application of NI-MH Batteries, NASA/TP, 2003, 211905.
[2] Y.H. Pan, V. Srinivasan, C.Y. Wang, J. Power Sources 112 (2002) 298–306.
[3] J. Shi, F. Wu, S. Chen, C. Zhang, J. Power Sources 157 (2006) 592–599.
[4] M.S. Wu, Y.Y. Wang, C.C. Wan, J. Power Sources 74 (1998) 202–210.
[5] B. Wu, M. Mohammed, D. Brigham, R. Elder, R.E. White, J. Power Sources 101 (2001) 149–157.
[6] W.B. Gu, C.Y. Wang, S.M. Li, M.M. Geng, B.Y. Liaw, Electrochim. Acta 44 (25) (1999) 4525–4541.
[7] S. Liu, R.A. Dougal, J.W. Weidner, J. Power Sources 141 (2005) 326–339.
[8] S.N. Lvov, D.D. Macdonald, J. Power Sources 72 (1998) 136–145.
[9] M.V. Quinzio, A.H. Zimmerman, Proceedings of the 17th Annual Conference on Applications and Advances, vol. 15, 2002, pp. 279–284.
[10] Schrage, S. Dean, Proceedings of the 26th Intersociety Energy Conversion Engineering Conference, vol. 3, 1991, pp. 21–44.